Rare Gas Quenching of Metastable O_2 ($b^1\Sigma_g^+$) at 295 K

Paul L. Kebabian† and Andrew Freedman*

Center for Chemical and Environmental Physics, Aerodyne Research, Inc., 45 Manning Road, Billerica, Massachusetts 01821-3976

Received: May 29, 1997[⊗]

The rare gas quenching rate constants of the metastable species, O_2 ($b^1\Sigma_g^+$), was measured using an induced fluorescence technique that utilizes an incoherent broadband light source and an integrating sphere to maximize excitation efficiency and fluorescence light collection. The measured rate constants at 295 K were the following (in units of 10^{-20} cm^3 molecule^{-1} s^{-1}): He, 430 ± 13; Ne, 26 ± 5; Ar, 9 ± 5; Kr, 32 ± 3; Xe, 67 ± 5. These values are of much lower magnitude than previous results indicate. However, except for that of helium, these rate constants should be regarded as upper limits, given that water vapor and hydrogen (both highly efficient quenchers) are ubiquitous contaminants of gas samples. The quenching rate constant with ground-state oxygen derived from these experiments, $(4.25 \pm 0.52) \times 10^{-17}$ cm^3 molecule s^{-1}, is in excellent agreement with previous results.

Introduction

The determination of the quenching rate constants of the O_2 ($b^1\Sigma_g^+$) metastable electronic state has received considerable attention because of the fact that the atmospheric oxygen A-band, O_2 ($X^3\Sigma_g^- \leftarrow b^1\Sigma_g^+$), is responsible for one of the most intense airglows in the terrestrial atmosphere.[1] This electronic state of oxygen also plays an important role in the energy-pooling processes that occur in the oxygen−iodine chemical laser.[2−4] Although accurate measurements of these rate constants have been made for major atmospheric constituents, only sketchy results are available for the rare gases He, Ne, Ar, Kr, and Xe.[1,5] These rate constants are quite small, and their accurate determination are hindered by the fact that the natural lifetime of this metastable state is so long (∼12 s)[6] and that water vapor and molecular hydrogen, ubiquitous contaminants of gas samples, are such efficient quenchers.[7]

Our interest in determining the quenching rate constants of this metastable species is due to our development of an oxygen Fraunhofer line discriminator (FLD) to be used for the ambient detection of chlorophyll fluorescence.[8] Green plants fluorescence in two bands centered at 740 and 680 nm, which happen to nearly coincide with the absorption maxima of the atmospheric oxygen A- and B-bands ($X^3\Sigma_g^- \rightarrow b^1\Sigma_g^+$, $v' = 0, 1$) respectively.[9,10] To maximize detection efficiency, a buffer gas (preferably one of the rare gases) must be added to the FLD to minimize diffusion to the cell walls and subsequent loss of metastable species by wall-induced quenching. Measurement of accurate quenching rate data is necessary to determine both the identity and optimum fill pressure of the buffer gas.

We have used an induced fluorescence technique utilizing a simple broadband incoherent light source and a highly reflective integrating sphere (which maximizes both excitation efficiency and fluorescent light detection) to measure the quenching rate constants of the rare gases with the O_2 ($b^1\Sigma_g^+$) metastable electronic state. By rigorous exclusion of water vapor from the measurement volume, we have been able to obtain results that are far more precise and of much lower magnitude than those obtained previously.

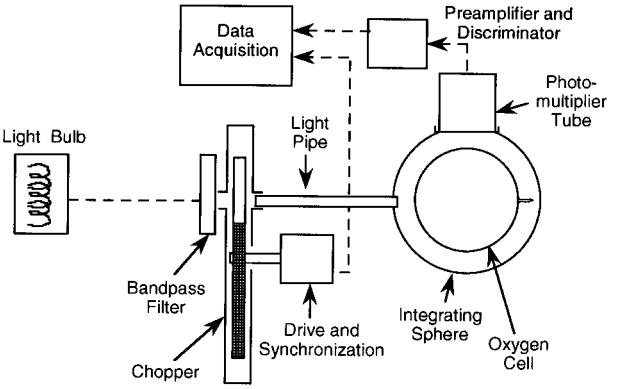

Figure 1. Schematic of oxygen fluorescence measurement apparatus.

Experimental Section

The induced fluorescence apparatus (shown in Figure 1) comprises an incandescent light source (a microscope illumination lamp), an interference filter centered at 760 nm (bandwidth of 10 nm), a chopping wheel, a 10 cm diameter quartz flask enclosed in a highly reflective (>99%) integrating sphere (Labsphere), a gated and cooled photomultiplier tube (EMI Model 9828), and a computer-controlled data acquisition system operated in a pulse-counting mode. Use of the integrating sphere provides for both uniform irradiation of the gas in the flask and for efficient collection of the induced fluorescence. During operation, 760 nm light irradiates the oxygen in the quartz cell while the chopper is open; the phototube is effectively disabled using the synchronization circuitry by lowering the voltage applied to the first few dynodes to reduce the effective current gain by several orders of magnitude. After the chopper blocks the light source, the phototube is turned on and the resulting fluorescence decay curve is generated by collecting the photocurrent-generated pulses in 2 ms long time bins. During the excitation phase, a silicon diode monitors the incident light intensity in the integrating sphere. A current-to-frequency converter changes this signal to a pulse train, which is acquired by a counter. This reference signal is used to normalize the detected photocurrent signal. Both phototube dark current (20−30 s^{-1}) and any residual fluorescence of the phototube envelope or internal structures are subtracted from the signals. We note

† Email: pkebab@aerodyne.com.
* To whom correspondence should be addressed. E-mail: af@aerodyne.com.
⊗ Abstract published in *Advance ACS Abstracts,* September 15, 1997.

S1089-5639(97)01728-3 CCC: $14.00

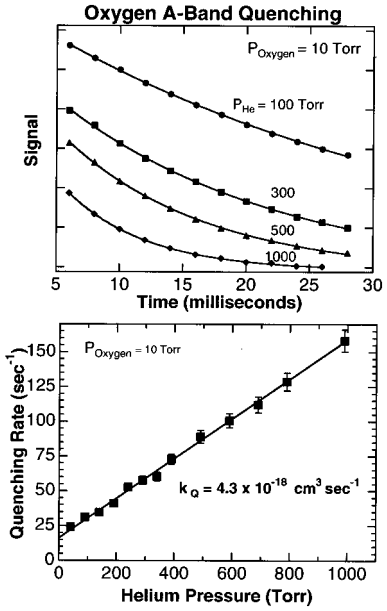

Figure 2. (Top panel) Time decay signals of oxygen fluorescence as a function of helium partial pressure. Nonlinear least squares fits to the data are shown as solid lines through the data points. (Bottom panel) First-order decay curve (Stern−Volmer plot) derived from the fits to the data shown above.

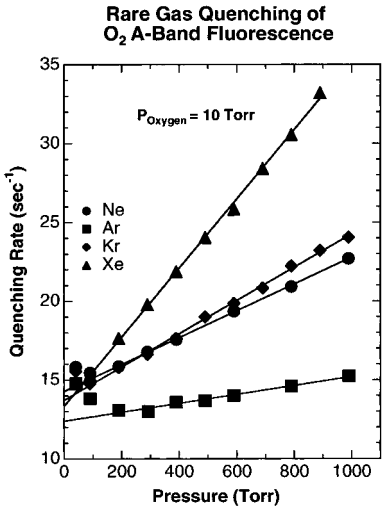

Figure 3. First-order decay quenching rate curves derived from time decay of fluorescence signal as a function of neon, argon, krypton, and xenon partial pressure. Solid curves are linear least squares fits to the data points. Note the upturn at low pressures caused by increased diffusion rates and subsequent wall-induced losses.

that the use of a quartz cell is mandatory, since both normal borosilicate and soda lime glasses fluoresce in this wavelength region.

The gases used in these experiments were of the following purity: He, 99.9999%; Ne, 99.9995%; Ar, 99.9995%; Kr, 99.995%; Xe, 99.995%; O_2, 99.994%. To further reduce the amount of water present in the system, all gases were passed through a cartridge filled with barium oxide, which acts as a desiccant. The gas line was constructed of stainless steel components and metal seals except for the connection to the quartz flask, which utilized a Viton O-ring seal. Both the gas line and quartz flask were subjected to bakeout at 100 °C for 24 h. The flask bakeout was carried out *ex situ* using a flow of dry air (dew point less than −60 °C) to prevent back-diffusion of ambient water vapor. Immediately before assembly, 75 mg of BaO was put into the bottom of the flask. Gas pressures were measured using capacitance manometers.

During a typical experiment, the quartz flask was filled with 10.0 Torr of oxygen and further backfilled with varying partial pressures of the rare gases. Time-dependent fluorescence signals were recorded with the light beam both on and off in order to allow for the subtraction of any photomultiplier tube dark current. The corrected signals were then averaged and fitted by an exponential function using a nonlinear least squares fitting routine to provide the fluorescence quenching rate (the natural fluorescence rate of the O_2 ($b^1\Sigma_g^+$) state is much smaller than any measured quenching rate). All experiments were performed at room temperature (295 ± 2 K).

Results and Discussion

Typical results of fluorescence decays as a function of buffer gas partial pressure are shown in the top panel of Figure 2 for helium. The fluorescence quenching rates determined from each partial pressure of helium were then plotted versus helium partial pressure (a Stern−Volmer plot) as shown in the bottom panel of Figure 2. The slope of the straight line provides the buffer gas quenching rate constant. The intercept of this line, corresponding to the absence of buffer gas, provides the quenching rate of the metastable state by oxygen itself at 10 Torr total pressure. Figure 3 provides similar Stern−Volmer plots for neon, argon, krypton, and xenon. The upturn in the measured fluorescence quenching rate at low partial pressures of the buffer gases is caused by the increase in diffusion rates and subsequent wall-induced quenching.

TABLE 1: Measured O_2 ($b^1\Sigma_g^+$) Quenching Rates at 295 K

gas	quenching rate (10^{-20} cm^3 molecule^{-1} s^{-1})	lit values
He	430 ± 13[a]	<1000,[7] <1000,[15] 25 000[5]
Ne	26 ± 5[a]	<10,000,[11] 36 000[5]
Ar	9 ± 5[a]	<580,[11] <1000,[15] 1500,[7] 47 000[5]
Kr	32 ± 3[a]	10 000,[11] 58 000[5]
Xe	67 ± 5[a]	~10 000,[11] 126 000[5]
O_2	4250 ± 520[b]	4000,[12] 3800,[13] 4600[14]

[a] Convolution of estimated experimental and data-fitting uncertainty. [b] Statistical uncertainty (95% confidence level) of five independent measurements.

The derived quenching rate constants of the O_2 ($b^1\Sigma_g^+$) state by the rare gases are reported in Table 1 along with estimated error limits. The error limits include contributions from statistical errors and known experimental uncertainties (2% accuracy for pressure measurements and 1% error due to temperature fluctuations). Systematic errors caused by sample contamination, for example, may be far larger in magnitude. Several previous measurements of the quenching rate constants are also listed for comparison.

The quenching rate constant of the O_2 ($b^1\Sigma_g^+$) state by ground-state oxygen itself can be obtained as well from the Stern−Volmer plots by dividing the intercepts obtained from the fits to the data by the partial pressure of oxygen (10 Torr). By determining the intercepts using various rare gases, we have five independent determinations of the oxygen quenching rate constant; the error limit of the value reported in Table 1 is 2.15 times the standard deviation of the mean (95% confidence level). The reported value is in excellent agreement with results from previous determinations.

The quenching rate constants for the rare gases obtained in these experiments are much lower than previously reported. We ascribe this to our success in maintaining a clean environment; most of the previous results reported in Table 1 are undoubtedly limited by the presence of a water impurity. The improbably high values reported in ref 5 are the result of the subtraction of

two large measured values and should be regarded with skepticism. The small magnitude of these quenching rate constants is reasonable in that, assuming that quenching to the spin-allowed $a^1\Delta$ state takes place,[16] the only operative mechanism is that of E → T transfer. However, it is probably prudent to regard the values recorded here for all the rare gas rate constants, except that of helium, as upper limits, since the obtained results are equivalent to the presence of only ∼20−140 ppb of water vapor and/or 160−1000 ppb of hydrogen in the rare gas fill.

The observed trend in the magnitude of the rate constants is surprising. Helium, although an inefficient quencher compared to molecular species, possesses a quenching rate constant 6−40 times that of the other rare gases. Even when these values are corrected to quenching cross section, helium, the smallest of all the rare gases, still exhibits the highest propensity for quenching the ($b^1\Sigma_g^+$) state of oxygen. This result is unexpected in that, given the absence of any strong chemical interaction, the magnitude of physical quenching of the oxygen excited state by a rare gas atom is naively expected to scale with atomic polarizability.

Acknowledgment. The authors acknowledge financial support from the National Aeronautics and Space Administration (John C. Stennis Space Center), Contract No. NAS13-707, under the Small Business Innovation Research Program.

References and Notes

(1) Wayne, R. P. *Singlet Oxygen*; Frimer, A. A., Ed.; CRC Press: Boca Raton, FL, 1985; Vol. 1, p 81.

(2) Ddyukov, A. I.; Kulagin, Y. A.; Shelepin, L. A.; Varygina, V. A. *Sov. J. Quantum Electron*. **1989**, *19*, 578.

(3) Aharon, O.; Elior, A.; Herskowitz, M.; Lebiush, E.; Rosenwaks, S. *J. Appl. Phys*. **1991**, *70*, 5211. Barmashenko, B. D.; Rosenwaks, S. *J. Appl. Phys*. **1993**, *73*, 1598.

(4) Endo, M.; Kodama, K.; Handa, Y.; And Uchiyama, T. *Appl. Phys. B* **1993**, *56*, 71.

(5) See, for example, data reviewed in the following. Shi, J.; Barker, J. R. *Int. J. Chem. Kin*. **1990**, *22*, 1283.

(6) Wallace, L.; Hunten, D. M. *J. Geophys. Res*. **1968**, *73*, 4813.

(7) Becker, K. H.; Groth, W.; Schurath, U. *Chem. Phys. Lett*. **1971**, *8*, 259.

(8) Kebabian, Paul L. Spectral Discriminator For Passive Detection Of Fluorescence. U.S. Patent 5,567,947, October 22, 1996.

(9) Lichtenhaler, H. K.; Rinderle, U. *CRC Crit. Rev. Anal. Chem., Suppl. 1* **1988**, *19*, S29.

(10) Mazzinghi, P. *Rev. Sci. Instrum*. **1996**, *67*, 3737.

(11) Filseth, S. V.; Zia, A.; Welge, K. H. *J. Chem. Phys*. **1970**, *52*, 5502.

(12) Martin, L. R.; Cohen, R. B.; Schatz, J. F. *Chem. Phys. Lett*. **1976**, *41*, 394.

(13) Lawton, S. A.; Novick, S. E.; Broida, H. P.; Philips, A. V. *J. Chem. Phys*. **1977**, *66*, 1381.

(14) Thomas, R. G. O.; Thrush, B. A. *J. Chem. Soc., Faraday Trans. 2* **1975**, *71*, 664.

(15) Wildt, J.; Bednarek, G.; Fink, E. H.; Wayne, R. P. *Chem. Phys*. **1991**, *156*, 497.

(16) Wildt, J.; Bednarek, G.; Fink, E. H.; Wayne, R. P. *Chem. Phys*. **1988**, *122*, 463.